Supporting Information for

Investigating the direct meltwater effect in terrestrial oxygen-isotope paleoclimate records using an isotope-enabled Earth system model

Jiang Zhu[1,2*], Zhengyu Liu[3], Esther C. Brady[4], Bette L. Otto-Bliesner[4], Shaun A. Marcott[5], Jiaxu Zhang[6], Xianfeng Wang[7], Jesse Nusbaumer[8], Tony E. Wong[9], Alexandra Jahn[10], and David Noone[11]

[1]Department of Atmospheric and Oceanic Sciences and Center for Climatic Research, University of Wisconsin-Madison, Madison, Wisconsin, USA
[2]Now at Department of Earth and Environmental Sciences, University of Michigan, Ann Arbor, Michigan, USA
[3]Atmospheric Science Program, Department of Geography, The Ohio State University, Columbus, Ohio, USA
[4]Climate and Global Dynamics Laboratory, National Center for Atmospheric Research, Boulder, Colorado, USA
[5]Department of Geoscience, University of Wisconsin, Madison, Wisconsin, USA
[6]*CCS-2 and CNLS, Los Alamos National Laboratory, Los Alamos, New Mexico, USA*
[7]Asian School of the Environment and Earth Observatory of Singapore, Nanyang Technological University, Singapore
[8]NASA Goddard Institute for Space Studies, New York, New York, USA
[9]Department of Computer Science, University of Colorado Boulder, Boulder, Colorado, USA
[10]Department of Atmospheric and Oceanic Sciences and Institute of Arctic and Alpine Research, University of Colorado Boulder, Boulder, Colorado, USA
[11]College of Earth, Ocean, and Atmospheric Sciences, Oregon State University, Corvallis, Oregon, USA

Contents of this file

Introduction

Supporting information includes climate response, time series, model-data comparison, the direct meltwater effect over the globe, and results from water tagging experiments

Corresponding author: Jiang Zhu, 1225 W. Dayton St., Madison, WI 53706. jzhu47@wisc.edu

Text S1. Response of the AMOC, Greenland Temperature and Eastern Brazil Precipitation

We provide the time series of the AMOC strength, changes of temperature averaged over Greenland, and precipitation averaged over eastern Brazil for all the experiments in Figure S1. In the preindustrial control simulation, the AMOC is stable and around 24 Sv. The AMOC weakens differently in response to the different meltwater forcing in the sensitivity experiments. The AMOC decreases to 17.5, 5.7, 2.8 and 2.6 Sv in response to 0.10-, 0.25-, 0.50- and 1.00-Sv meltwater in the northern North Atlantic Ocean, respectively. It shows that 0.25-Sv meltwater (as used in experiment WH025a) can almost shutdown the AMOC by weakening it by 76% in 100 years. Another 0.25-Sv of meltwater (WH050a) further weakens the AMOC by 88% of its original strength. Meltwater discharged into the Gulf of Mexico also substantially weakens the AMOC, but at a slower rate than meltwater in the northern North Atlantic. Meanwhile, meltwater forcing of 0.50 Sv in the Weddell Sea only reduces the AMOC strength slightly by 1.9 Sv (8%) in 100 years.

Along with the weakened AMOC, the average temperature in Greenland decreases correspondingly in the water hosing experiments. However, there is a limit to the temperature decrease. The cooling over Greenland in 100 years reaches a maximum of ~9 °C when the meltwater forcing is 0.25 Sv, and more meltwater does not lead to further cooling. We find that this is due to an almost collapsed AMOC in WH025a, so that the reduction of the northward heat transport is already at its maximum. In all the water hosing experiments with meltwater discharged in the Northern Hemisphere, precipitation in eastern Brazil increases as a result of the southward shift of the ITCZ. Generally, the more the AMOC strength decreases, the more the precipitation in eastern Brazil increases. Meltwater discharged into the Weddell Sea does not alter the eastern Brazil precipitation by much.

Text S2. Changes of Surface Air Temperature, Precipitation and Surface $\delta^{18}O$ of Seawater in WH025a

The annual mean surface air temperature, precipitation and the surface $\delta^{18}O$ of seawater in the preindustrial control simulation and the changes in 100 years in the water hosing experiment with 0.25-Sv meltwater into the northern North Atlantic (WH025a) are shown in Figure S2. As a result of the associated reduced northward oceanic heat transport, the surface air temperature exhibits the expected bipolar seesaw response [*Broecker*, 1992]. The Northern Hemisphere cools by an average of 3.7 ºC, with a maximum cooling exceeding 20 ºC in the northern North Atlantic in the first 100 years. Simultaneously, the Southern Hemisphere warms by an average of 0.1 ºC, with a maximum warming of about 1.0 ºC in the mid-latitudes.

Along with the "bipolar seesaw", the ITCZ shifts southward in the Indian Ocean, the eastern Pacific Ocean and the Atlantic Ocean, as is shown in the migration of the equatorial rainfall bands. At the same time, there are indications of weakened Northern Hemisphere monsoons, including the East Asia Monsoon, South Asian Monsoon and North Africa Monsoon and intensified Southern Hemisphere monsoons. The surface $\delta^{18}O$ in seawater ($\delta^{18}O_{sw}$) over the northern North Atlantic ranges from -2 to 0.4 ‰ in the preindustrial control simulation, which is much more enriched compared to the freshwater (-30 ‰) added in the water hosing experiments. As a result, $\delta^{18}O_{sw}$ decreases by about 3–4 ‰ over the northern North Atlantic and by about 1–2 ‰ over the subtropical Atlantic and the Arctic in the first 100 years in WH025a.

Text S3. Model $\delta^{18}O$ Compared with Reconstructions

The experiment WH025a can capture the abrupt changes in $\delta^{18}O_p$ of about 5 ‰ in Greenland ice core records during Heinrich events [e.g., *Johnsen et al.,* 2001]. Model simulated responses in low-latitude $\delta^{18}O$ in water hosing experiments (WH025a and

WH050a) are compared with cave records compiled by *Lewis et al.* [2010] in Figure S3. We also added a new record by *Stríkis et al.* [2015]. We have included the effect from temperature changes using the equation from *Kim and O'Neil* [1997]. The model results in WH025a and WH050a can well reflect the values in speleothem records with an overall correlation coefficient of 0.8 and 0.9, respectively. The model can reproduce the increased $\delta^{18}O_c$ in East Asia and decreased values in eastern Brazil remarkably well. We are aware that other complicated cave hydrological and geochemical processes can still impact stalagmite $\delta^{18}O$ and complicate the model-data comparison [*Fairchild et al.*, 2006]. Also, details of past meltwater events are poorly constrained in paleoclimate records and our water hosing experiments are intended to be highly idealized. Therefore, necessary caution should be taken when comparing $\delta^{18}O$ in the model with these speleothem records.

Text S4. The Direct Meltwater Effect over the Globe

The total changes of the $\delta^{18}O_p$, the contribution by the direct meltwater effect and the direct meltwater effect in percentage in the last 30 years in the WH025a experiment are shown in Figure S4. The direct meltwater effect is the largest in the northern North Atlantic, indicating its role as the dominant local moisture source. The ^{18}O-depleted signal from the meltwater can propagate to nearby regions including Greenland, the Arctic, Eurasia, North Africa and Central America. The direct meltwater effect is around 15% of the total $\delta^{18}O$ response in Greenland, more than 50% in Europe, and about 35% in eastern Brazil. In particular, relative to the climatic effect, the direct meltwater effect becomes more important downstream into the Eurasian continent, as seen in a clear tongue of high percentage of direct effect extending from the North Atlantic well into the high latitude of Eurasian Continent, and this tongue is much clear than in the total and direct $\delta^{18}O_p$ signal themselves. This is perhaps an indication of the more advective nature of the direct meltwater effect than the climatic effect, the latter could be distorted by

atmospheric stationary waves and other processes. Interestingly, for some regions the direct meltwater effect can be in the opposite sign to the climate effect. For example, over East and South Asia, the $\delta^{18}O_p$ increase caused by the climate effect is slightly offset by the decrease from the direct meltwater effect. This suggests that a quantitative interpretation of oxygen-isotope records there could underestimate the monsoon changes by about 5–10% during meltwater events if the direct meltwater effect is not considered.

The sensitivity of the direct meltwater effect to locations of freshwater forcing (0.50 Sv lasting 100 years) is shown in Figure S5. In the experiment WH050a (discharging 0.50-Sv meltwater into the northern North Atlantic), the spatial pattern of the direct meltwater is comparable to WH025a, but the magnitude is generally larger. Adding freshwater forcing into the Gulf of Mexico (WH050b) produces a similar result as WH050a. The modelling experiment WH050c shows that adding meltwater into the Weddell Sea does not generate large changes in total $\delta^{18}O_p$ over both Greenland and eastern Brazil. Therefore, the meltwater effect there is trivial. It should also be noted that the region of the greatest influence of the direct meltwater effect for meltwater discharges into the Gulf of Mexico and Antarctic could differ significantly from that of melting water discharge into the North Atlantic. So, their impact on some regions other than Greenland and Northeast Brazil could become even greater than their effect on Greenland and Northeast Brazil as shown in Figure 2.

Text S5. Moisture Source Regions for Precipitation in Greenland and Eastern Brazil

We conducted an additional water tagging experiment to investigate the moisture sources for Greenland and eastern Brazil precipitation. In the tagging experiment, moisture from a certain region is tagged such that its movement in the hydrological cycle is tracked. In this experimental setup, the globe is divided into small regions, including land, the Southern Ocean, the northern North Atlantic, northern North Pacific, subtropical

North Atlantic, subtropical North Pacific, equatorial Atlantic, equatorial Pacific, subtropical South Atlantic Arctic, etc. The moisture fluxes from these individual regions are tracked in the tagging experiment. The tagging experiments are run in an atmosphere-only configuration, and the surface boundary conditions are from the preindustrial control and WH025a simulations, respectively.

The percentage of Greenland and eastern Brazil precipitation originating from different parts of the Atlantic Ocean in the water tagging experiment is shown in Table S1. More than half of the Greenland precipitation originates from the northern North Atlantic, and 7% comes from the subtropical Atlantic. Changes of $\delta^{18}O$ in seawater over these regions could reach -3 and -1 ‰ in 300 years in experiment WH025a (Figure S2). For eastern Brazil, about 15% of its precipitation comes from the subtropical North Atlantic and the equatorial Atlantic; changes of $\delta^{18}O$ in seawater there can reach about 0.4 ‰ with maximum exceeding -1‰ (Figure S2) in 300 years.

	Northern N. Atl. (30–70°N)	Subtropical N. Atl. (10–30°N)	Equatorial Atl. (10°S–10°N)	Subtropical S. Atl. (10-30°S)
Contribution to Greenland precipitation	51% (31%)	7% (10%)	<1% (<1%)	<1% (<1%)
Contribution to eastern Brazil precipitation	1% (1%)	2% (5%)	13% (20%)	50% (39%)

Table S1. Percentage of Greenland and eastern Brazil precipitation that originates from the different parts of the Atlantic Ocean in the preindustrial control and WH025a (in parentheses) simulations
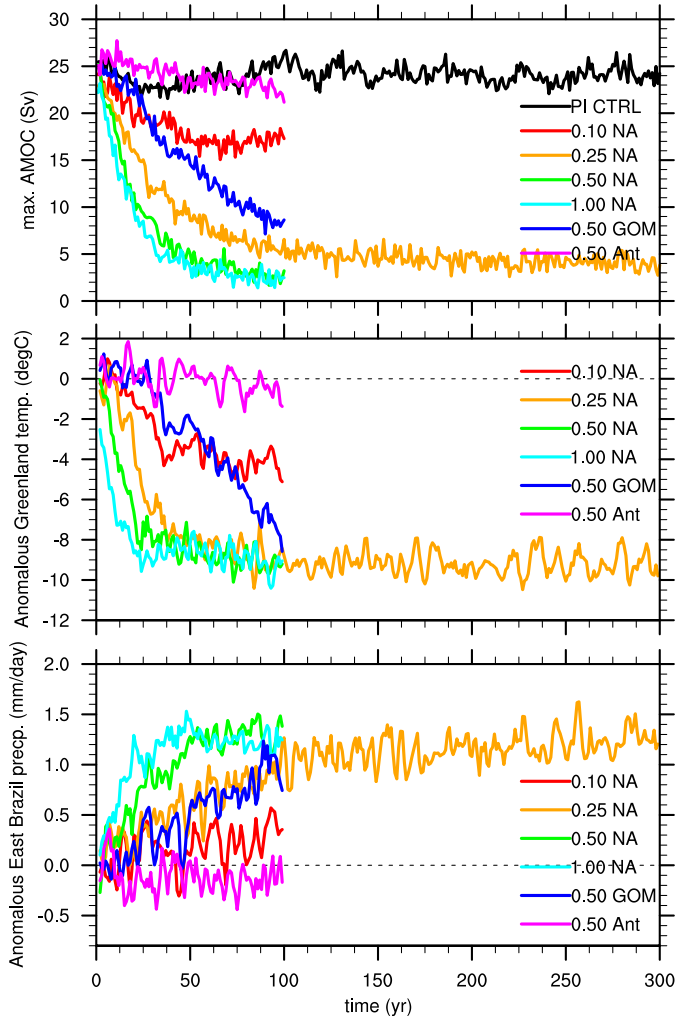
Figure S1. Time series of the AMOC maximum strength in the North Atlantic (top), the anomalous annual mean Greenland temperature (middle) and the anomalous annual mean precipitation in eastern Brazil (bottom) in the preindustrial control and the water hosing sensitivity experiments.
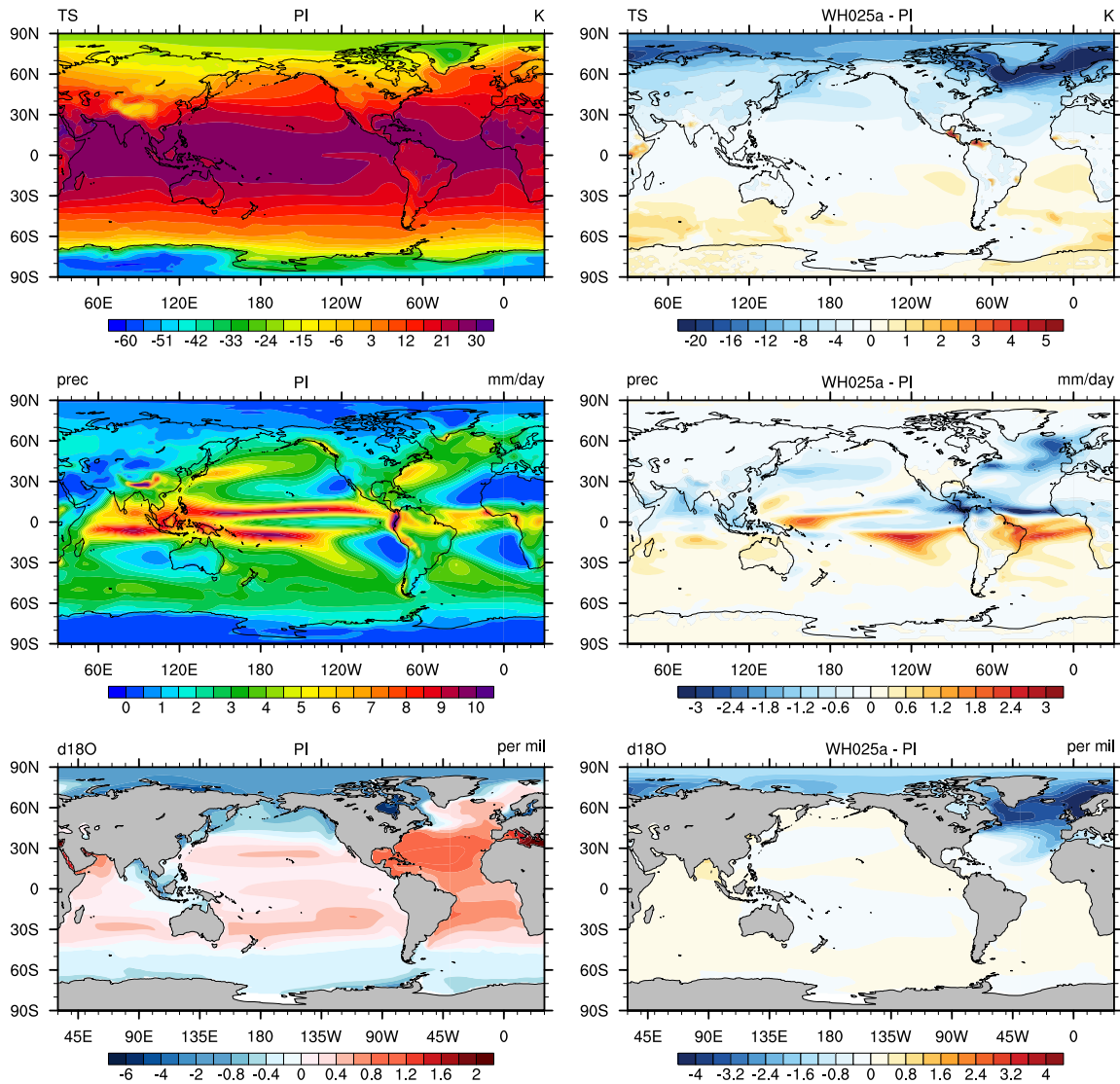
Figure S2. Annual mean surface temperature (top, left), precipitation (middle, left) and the $\delta^{18}O$ of surface seawater (VSMOW, bottom, left) in the preindustrial control simulation and the changes (right) in 100 years in the WH025a experiment.
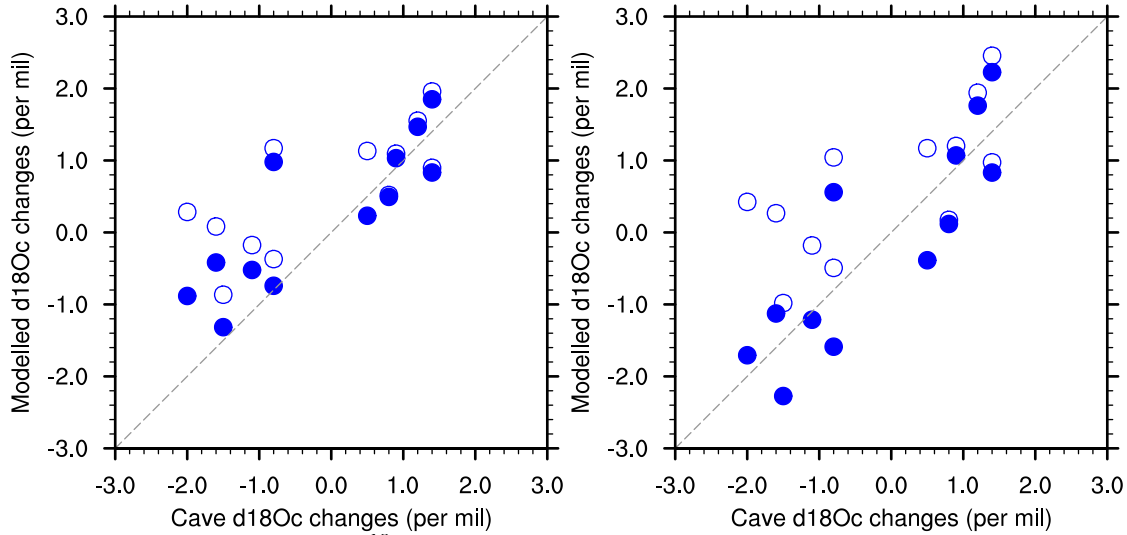
Figure S3. The stalagmite δ^{18}O$_c$ responses during Heinrich events (compiled by *Lewis et al.* [2010]; Also added *Stríkis et al.* [2015]; x-axis) compared with model simulated changes in δ^{18}O$_c$ in WH025a (left) and WH050a (right). Modelled δ^{18}O$_c$ is calculated from model δ^{18}O$_p$ and temperature using *Kim and O'Neil* [1997]. Open circles are results if only the indirect climate effects are considered (experiments WH025aC and WH050aC). The cave records and the corresponding Heinrich events are, from left to right, Poleva Cave (44°43'N, 21°45'E; H4; *Constantin et al.,* 2007), Rio Grande do Norte (5°36'S, 37°44'W; H1, H2; *Cruz et al.,* 2009), Lapa Sem Fim Cave (16°09′S, 44°37′W; H1; *Stríkis et al.,* 2015), Botuverá Cave (27°13'S, 49°9'W; H1–H5; *Wang et al.,* 2006; *Cruz et al.,* 2006), Santana Cave(24°32'S, 48°44'W; H1, H3–H6; *Cruz et al.,* 2006), Cave of the Bells (31°45'N, 110°45´E; H4; *Wagner et al.,* 2010), Soreq Cave (31°27'N, 35°02'E; H1, H2, H5; *Bar-Matthews et al.,* 1999), Borneo (4°12'N,114°56'E; H1; *Partin et al.,* 2007), Moomi Cave (12°30'N, 54°E; H1, H5; *Shakun et al.,* 2007); Sanbao Cave (31°40´N, 110°26´E; H1; *Wang et al.,* 2008); Songjia Cave (32°25′N, 107°11′E; H1; *Zhou et al.,* 2008), Hulu Cave (32°30′N, 119°10′E; H1–H4; *Wang et al.,* 2001).
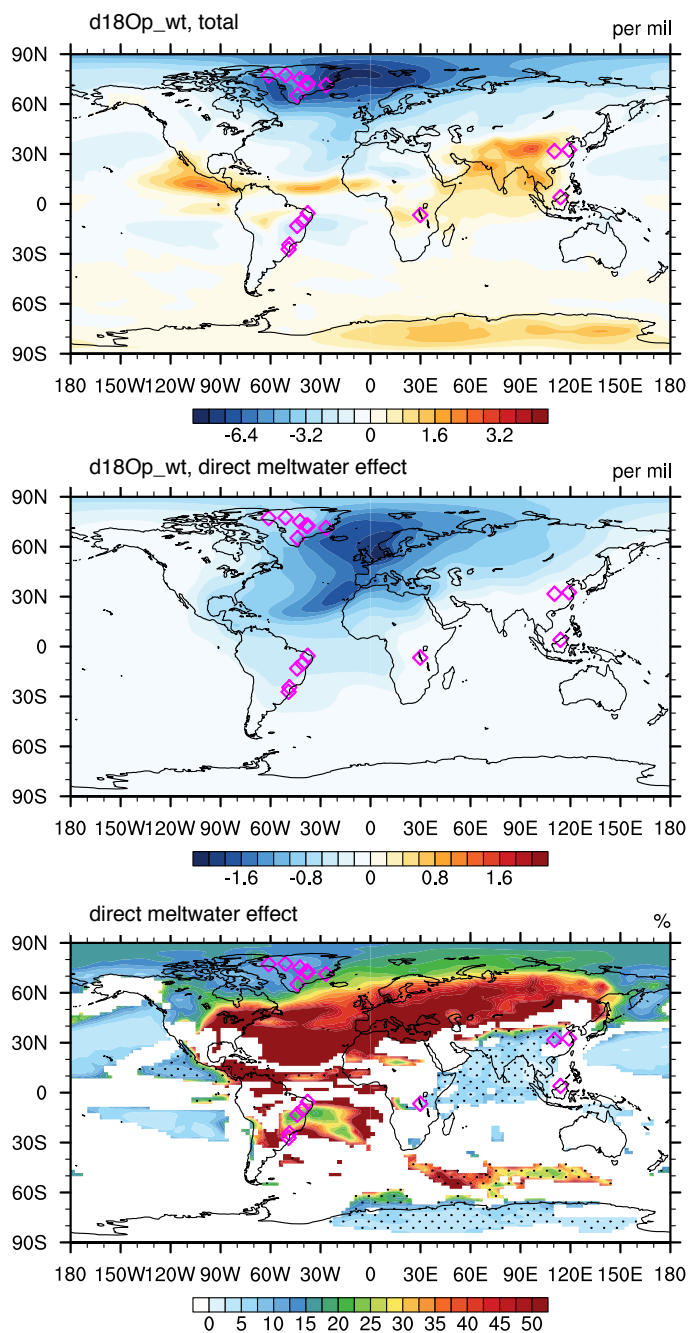
Figure S4. The total changes in δ^{18}O in precipitation (VSMOW, top), the direct meltwater effect (middle) and the direct meltwater effect in percentage (bottom) averaged between 271 to 300 years in the WH025a experiment. In the bottom figure, only regions with total changes larger than the internal variability (one standard deviation) are filled. Regions with the direct meltwater effect opposite to the total changes are dotted. Markers in the map denote locations of related oxygen-isotope records in the literature.
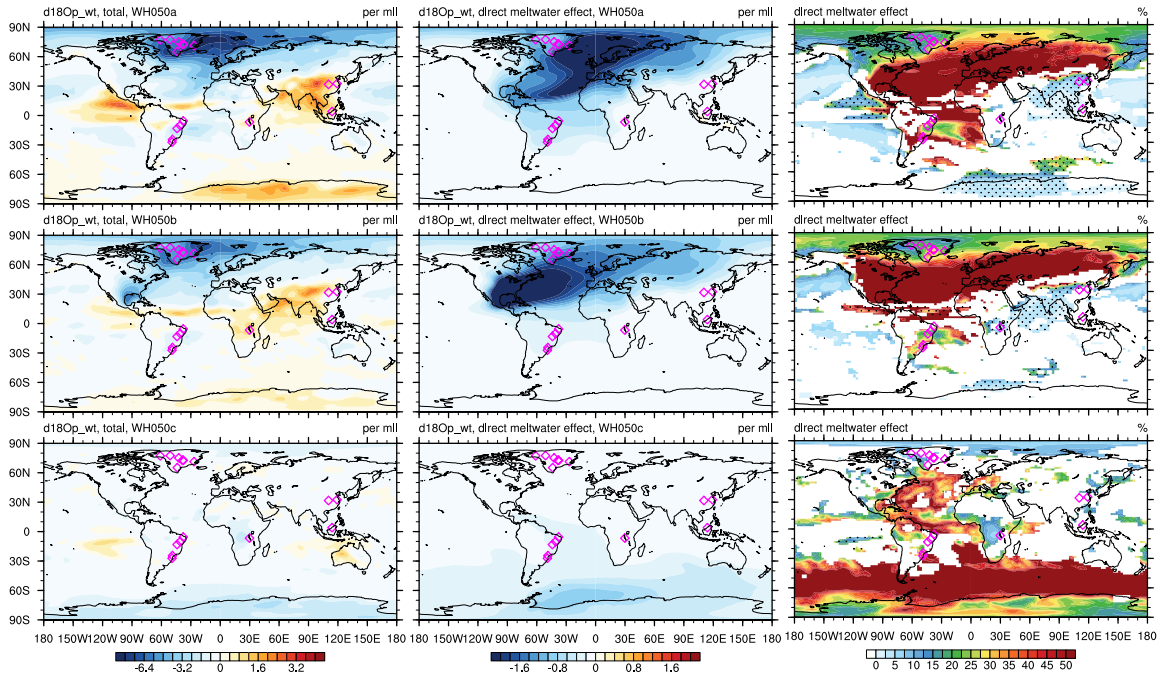
Figure S5. The total changes in 100 years in $\delta^{18}O$ in precipitation (VSMOW, left column), the direct meltwater effect (middle column) and the direct meltwater in percentage (right column) in the experiments with 0.50-Sv meltwater discharged into the northern North Atlantic (top row), the Gulf of Mexico (middle row) and the Weddell Sea (bottom row). In figures in the right column, only regions with total changes larger than the internal variability (one standard deviation) are filled. Regions with the direct meltwater effect opposite to the total changes are dotted. Markers in the map denote locations of related oxygen-isotope records in the literature.